Computers, Materials & Continua CMC, vol.64, no.2, pp.1219-1232, 2020

Image Denoising with Adaptive Weighted Graph Filtering

Ying Chen[1, 2], Yibin Tang[3], Lin Zhou[1], Yan Zhou[3, 4], Jinxiu Zhu[3] and Li Zhao[1, *]

Abstract: Graph filtering, which is founded on the theory of graph signal processing, is proved as a useful tool for image denoising. Most graph filtering methods focus on learning an ideal lowpass filter to remove noise, where clean images are restored from noisy ones by retaining the image components in low graph frequency bands. However, this lowpass filter has limited ability to separate the low-frequency noise from clean images such that it makes the denoising procedure less effective. To address this issue, we propose an adaptive weighted graph filtering (AWGF) method to replace the design of traditional ideal lowpass filter. In detail, we reassess the existing low-rank denoising method with adaptive regularizer learning (ARLLR) from the view of graph filtering. A shrinkage approach subsequently is presented on the graph frequency domain, where the components of noisy image are adaptively decreased in each band by calculating their component significances. As a result, it makes the proposed graph filtering more explainable and suitable for denoising. Meanwhile, we demonstrate a graph filter under the constraint of subspace representation is employed in the ARLLR method. Therefore, ARLLR can be treated as a special form of graph filtering. It not only enriches the theory of graph filtering, but also builds a bridge from the low-rank methods to the graph filtering methods. In the experiments, we perform the AWGF method with a graph filter generated by the classical graph Laplacian matrix. The results show our method can achieve a comparable denoising performance with several state-of-the-art denoising methods.

Keywords: Graph filtering, image denoising, Laplacian matrix, low rank.

1 Introduction

Image denoising plays an important role in various image processing and computer vision scenarios [Wu, Li, Lin et al. (2018); Chen, Wang, Liu et al. (2019)]. It is viewed as an inverse problem that clean images are restored from noisy ones [Buades, Coll and Morel (2005); Shao, Yan, Li et al. (2017)]. Though a huge number of denoising methods have been presented in past decades, they are mainly grouped in two categories, i.e., model-

[1] School of Information Science and Engineering, Southeast University, Nanjing, 210096, China.

[2] Department of Psychiatry and Translational Imaging, Columbia University & NYSPI, New York, 10032, USA.

[3] College of Internet of Things Engineering, Hohai University, Changzhou, 213022, China.

[4] Changzhou Key Laboratory of Sensor Networks and Environmental Sensing, Changzhou, 213022, China.

[*] Corresponding Author: Li Zhao. Email: zhaoli@seu.edu.cn.

Received: 15 March 2020; Accepted: 20 April 2020.

based and discriminative-learning-based methods. Most model-based methods handle the denoising problem only from the noisy image itself, where internal prior of image is exploited by various signal models. Meanwhile, discriminative-learning-based denoising methods pay more attention on external prior from different image databases. Many deep learning algorithms [Zhang, Zuo, Chen et al. (2016); Zhang, Zuo and Zhang (2018); Jia, Liu, Feng et al. (2019); Wang, Jiang, Luo et al. (2019)] are employed in the discriminative-learning-based methods, which significantly improve the quality of restored images. It proves that feature learning from external images is helpful for image denoising. Their remarkable performances benefit from the use of feature similarity between target image and external images. However, once target image and external images are mismatched, these methods become ineffective. In this case, the model-based methods show their advantage and still work well for denoising. Therefore, we focus on the model-based methods in this paper to restore images without the help of external images.

To our knowledge, model-based denoising methods are carried out in three domains, i.e., spatial, transform and learned domains. The spatial-domain denoising methods, e.g., bilateral filtering [Zhang and Gunturk (2008)] and non-local means approach [Verma and Pandey (2017)], estimate pixels or patches by fusing the neighborhood ones with similar structures. From the view of filtering, they use a spatial smoothing filter to remove the noise-like components of image. The transform-domain methods contribute to enhancing the denoising performance in other domains rather than the spatial domain. Generally speaking, they firstly decompose noisy images into a set of component coefficients on the bases in a transform domain such as wavelet and curvelet domains [Yan, Shao and Liu (2013); Tessens, Pizurica, Alecu et al. (2008); Deivalakshmi; Palanisamy and Gao (2019)]. Then denoised images are reconstructed by the shrinkage of their high-frequency component coefficients. Here, a method named as block matching and three-dimensional filtering (BM3D) [Dabov, Foi, Katkovnik et al. (2007); Mäkinen, Azzari and Foi (2019)] is preferred as a landmark for image denoising. It restores images from both spatial and transform domains, where Wiener and wavelet filters are sequentially adopted to extract the reliable components from similar patches.

As for image denoising in learned domain, it is dedicated to adaptively learn internal prior of target image for image restoration. Numerous methods via sparse representation [Liu, Chen, Chen et al. (2017); Wang, Cai, Shi et al. (2015)] and low rank approximation [Huang, Dong, Xie et al. (2017); Wang, Cen, He et al. (2018)] are presented with their impressive denoising performance. For sparse representation, image patches are efficiently described by a linear combination of atoms from a learned dictionary. Most sparse representation methods, e.g., K-means singular value decomposition [Elad and Aharon (2006)] and nonlocally centralized sparse representation (NCSR) [Dong, Zhang, Shi et al. (2013)], consider the sparsity of patches for denoising. But recent work shows the residual of patches has the sparsity attribute, which is also suitable for sparse representation to improve the denoising performance [Zha, Zhang, Wang et al. (2018)]. In another line of learned-domain methods, many low rank approximation approaches are developed by introducing the nuclear norm minimization (NNM) model [Zhang, He, Zhang et al. (2014)]. In the NNM model, it demonstrates that similar patches have their low rank attribute with the sparse singular values. Subsequently, a weighted NNM (WNNM) model and its extended version, low rank approximation with adaptive regularizer learning (ARLLR), are

presented to effectively shrink the singular values of patches [Jia, Feng and Wang (2016a, 2016b)], which make a great success in image denoising. Besides, various additional regularizers are adopted in the NNM model to employ other attributes of patches. For example, a regularizer of inter-patch correlation is recently utilized to reach a higher quality of denoised image [Liu, Xiong, Liu et al. (2018)].

On the other hand, graph signal processing has been rapidly developed in recent years. It is founded on the geometric structures of signals with the description of graph Laplacian matrix [Hein, Audibert and von Luxburg (2005)]. Meanwhile, graph-filtering-based methods are paid increasing attention to solve the image denoising problem, since noisy patches can contact with each other to form a graph. Several graph polynomial filtering methods are presented to employ various Laplacian matrix regularizers in the denoising model [Zeng, Bian, Liu et al. (2015); Pang and Cheung (2017); Waheed and Tay (2018)]. Graph filtering is also performed on noisy images for its advantage of graph frequency analysis. The existing graph filtering methods [Meyer and Shen (2014); Talebi and Milanfar (2014)] prove that the eigenvectors of graph Laplacian matrix of patches not only represent the global structures of image, but also can be utilized as a set of bases to reconstruct clean images. They have achieved the competitive denoising performance with BM3D. It is worth noting that these graph filtering methods all employ an ideal lowpass graph filter to remove noise, which restore clean images only with the image components in low graph frequency bands. This ideal filter has limited ability to separate the low-frequency noise from clean images such that it seriously hinders the performance of graph filtering.

To address the problem in graph filtering, an adaptive weighted graph filtering (AWGF) method is proposed for denoising. In detail, we firstly analysize the ARLLR model and treat it as a special form of graph filter. Then an adaptive shrinkage algorithm is presented for graph filtering by introducing the shrinking mechanism of ARLLR. To deal with a group of similar patches, the component in each graph frequency band is shrunk with its component significance. Consequently, it can remove the noise in all bands to overcome the drawback of traditional ideal lowpass graph filter. Experiments show the proposed method can effectively restore clean images. It achieves a comparable denoising performance with other state-of-the-art methods.

2 Related work

Some related work is given to better introduce our AWGF method. In this section, the denoising mechanisms of low rank approximation and graph filtering are respectively provided with more details.

2.1 Low rank approximation

The image denoising methods with low rank approximation can be generalized into an optimization problem as

$$\left\{\tilde{\sigma}_{x,i}\right\} = \arg\min_{\{\sigma_{x,i}\}} \frac{1}{2\tau}\left\|\boldsymbol{Y} - \boldsymbol{U}\boldsymbol{\Sigma}_x\boldsymbol{V}^T\right\|_F^2 + \sum_{i=1}^{r} g\left(\sigma_{x,i}\right), \tag{1}$$

where τ is the weighted coefficient, $\boldsymbol{Y}$ and $\boldsymbol{X}$ are the noisy and denoised patch groups,

the singular value decompositions of $\boldsymbol{Y}$ and $\boldsymbol{X}$ are respectively represented as $\boldsymbol{Y}=\boldsymbol{U}\boldsymbol{\Sigma}_y\boldsymbol{V}^T$ and $\boldsymbol{X}=\boldsymbol{U}\boldsymbol{\Sigma}_x\boldsymbol{V}^T$. Here, $\{\sigma_{y,i}\}$ and $\{\sigma_{x,i}\}$ are the corresponding diagonal entries of $\boldsymbol{\Sigma}_y$ and $\boldsymbol{\Sigma}_x$, and $g(\sigma_{x,i})$ is the prior regularizer of $\sigma_{x,i}$.

For the low rank model in Eq. (1), various prior regularizers have been proposed to increase the sparsity of singular values of $\{\sigma_{x,i}\}$. The traditional regularizers are set by the rank-based functions [Zhang, He, Zhang et al. (2014); Jia, Feng and Wang (2016b)]. However, the singular values are often over punished under the rank-based functions, which causes the lower denoising performance. More convex and non-convex functions are suggested as the prior regularizer [Hu, Zhang, Ye et al. (2013); Yang, Yang and Han (2018); Yang, Fan, Yang et al. (2019)]. Among them, the aforementioned ARLLR model that uses a logarithm function as its regularizer becomes attractive. It not only well explains the low rank model in the Bayesian framework, but also achieves the better denoising performance than other existing low rank methods. Its optimization problem is described as

$$\{\tilde{\sigma}_{x,i}\}=\arg\min_{\{\sigma_{x,i}\}}\frac{1}{2\tau}\left\|\boldsymbol{Y}-\boldsymbol{U}\boldsymbol{\Sigma}_x\boldsymbol{V}^T\right\|_F^2+\sum_{i=1}^{r}log\left|\sigma_{x,i}+\varepsilon\right|, \tag{2}$$

where the prior regularizer is defined as a covex non-linear function, $g(\sigma_{x,i})=log\left|\sigma_{x,i}+\varepsilon\right|$, and ε is a small positive constant.

2.2 Graph filtering

In the traditional graph filtering methods, denoised images are achieved by an ideal lowpass filter in the graph frequency domain. Therefore, these methods are essentially the transform-domain methods. The design of transform bases now becomes an important step for filtering. Given a graph Laplacian matrix $\boldsymbol{L}$ to describe the graph structure of N patches, the eigenvectors of $\boldsymbol{L}$ are provided as $\boldsymbol{V}_g=\left[\boldsymbol{v}_{g,1},\boldsymbol{v}_{g,2},\cdots,\boldsymbol{v}_{g,N}\right]$ with the ascending eigenvalues. The bases of lowpass graph filter is thus obtained with the first M eigenvectors as $\boldsymbol{V}_g^{lp}=\left[\boldsymbol{v}_{g,1},\boldsymbol{v}_{g,2},\cdots,\boldsymbol{v}_{g,M}\right]$. The graph filtering procedure for patches can be simply written as

$$\boldsymbol{X}=\boldsymbol{Y}\boldsymbol{V}_g^{lp}\left(\boldsymbol{V}_g^{lp}\right)^T, \tag{3}$$

In Eq. (3), the denoised patch group $\boldsymbol{X}$ is restored by retaining the low-frequency components of noisy patch group $\boldsymbol{Y}$. It also indicates the filtering performance depends on the basis number M. Several eigenvector selection approaches are proposed to estimate the number M adaptively under the control of image noise [Chen, Tang, Xu et al. (2016); Tang, Chen, Xu et al. (2016)]. Unfortunately, these methods still belong to the ideal lowpass graph filtering methods.

3 Proposed method

Motivated by recent process, we propose an adaptive weighted graph filtering method for image denoising. Moreover, the explanation of graph filtering is also given to the existing ARLLR method and uniforms it in the proposed method.

3.1 Adaptive weighted graph filtering

We present an adaptive weighted graph filtering in this section. The AWGF model is firstly given as

$$\left\{\tilde{\sigma}_{g,i}\right\} = \arg\min_{\{\sigma_{g,i}\}} \frac{1}{2\tau}\left\|\boldsymbol{Y} - \boldsymbol{Y}\boldsymbol{V}_g\boldsymbol{\Sigma}_g\boldsymbol{V}_g{}^T\right\|_F^2 + \sum_{i=1}^{N} g\left(\sigma_{g,i}\right), \tag{4}$$

where the shrinkage coefficients $\left\{\sigma_{g,i}\right\}$ are the diagonal entries of matrix $\boldsymbol{\Sigma}_g$. Different from the traditional graph filtering of Eq. (3), all graph eigenvectors of $\boldsymbol{V}_g$ are used as the filter bases in Eq. (4). Thus, the noisy patch group $\boldsymbol{Y}$ can be well represented in the full space supported by bases $\boldsymbol{V}_g$. The denoised patch group $\boldsymbol{X}$ is obtained as

$$\boldsymbol{X} = \boldsymbol{Y}\boldsymbol{V}_g\boldsymbol{\Sigma}_g\boldsymbol{V}_g^T, \tag{5}$$

Inspired by ARLLR, a similar prior regularizer is set as $g\left(\sigma_{g,i}\right) = log\left|\beta_i\sigma_{g,i} + \varepsilon\right|$ with the weighted coefficient β_i. Substituting $g\left(\sigma_{g,i}\right)$ to Eq. (4), we describe the AWGF model in a trace form as

$$\left\{\tilde{\sigma}_{g,i}\right\} = \arg\min_{\{\sigma_{g,i}\}} \frac{1}{2\tau} trace\left(\boldsymbol{Y}\boldsymbol{V}_g\left(\boldsymbol{I} - \boldsymbol{\Sigma}_g\right)^2\boldsymbol{V}_g{}^T\boldsymbol{Y}^T\right) + \sum_{i=1}^{N} log\left|\beta_i\sigma_{g,i} + \varepsilon\right|, \tag{6}$$

Sequentially, problem Eq. (6) can be separated into a set of sub-problems by defining the matrix $\boldsymbol{P} = \boldsymbol{Y}\boldsymbol{V}_g$ with its vectors $\{\boldsymbol{p}_i\}$ as

$$\tilde{\sigma}_{g,i} = \arg\min_{\sigma_{g,i}} \frac{1}{2\tau} trace\left(\boldsymbol{p}_i\left(1-\sigma_{g,i}\right)^2\boldsymbol{p}_i^T\right) + log\left|\beta_i\sigma_{g,i} + \varepsilon\right|, \tag{7}$$

We rewrite Eq. (7) into a more simple formula as

$$\tilde{\sigma}_{g,i} = \arg\min_{\sigma_{g,i}} \frac{1}{2\tau}\left(\gamma_{y,i} - \gamma_{y,i}\sigma_{g,i}\right)^2 + log\left|\beta_i\sigma_{g,i} + \varepsilon\right|, \tag{8}$$

where $\gamma_{y,i}^2 = \boldsymbol{p}_i^T\boldsymbol{p}_i$ represents the component energy of $\boldsymbol{Y}$ on the basis $\boldsymbol{v}_{g,i}$. Here, we experientially set $\beta_i = \gamma_{y,i}$ and thus turn Eq. (8) into the final expression as

$$\tilde{\sigma}_{g,i} = \arg\min_{\sigma_{g,i}} \frac{1}{2\tau}\left(\gamma_{y,i} - \gamma_{y,i}\sigma_{g,i}\right)^2 + log\left|\gamma_{y,i}\sigma_{g,i} + \varepsilon\right|, \tag{9}$$

For problem Eq. (9), it has a closed form solution as

$$\tilde{\sigma}_{g,i} = \frac{1}{\gamma_{y,i}}\max\left(\gamma'_{y,i} - \frac{2\tau'_{y,i}}{\sqrt{\gamma'^2_{y,i} - 4\tau'_{y,i}}}, 0\right), \tag{10}$$

where $\gamma'_{y,i} = \gamma_{y,i} - \varepsilon$ and $\tau'_{y,i} = \tau - \varepsilon\gamma_{y,i}$. So far, the AWGF method completes the coefficient shrinkage procedure, where the denoised patch group $\boldsymbol{X}$ is consequently achieved by Eq. (5) with assembling $\boldsymbol{\Sigma}_g$ by $\left\{\tilde{\sigma}_{g,i}\right\}$.

We further propose an iterative AWGF framework for image denoising. As shown in **Algorithm 1**, the intermediate noisy image $\mathbf{Y}^{(k)}$ is tackled in the *k*-th iteration. In detail,

for the target patch group $\boldsymbol{Y}_j$ of $\mathbf{Y}^{(k)}$, its noise variance $\sigma_{n,j}$ is firstly estimated by

$$\sigma_{n,j} = \sqrt{\max\left(\sigma_n^2 - var\left(\boldsymbol{Y}_j - \boldsymbol{Y}_j'\right), 0\right)}, \tag{11}$$

where $\boldsymbol{Y}_j'$ is the patch group of noisy image $\mathbf{Y}$ sharing the same patch index of $\boldsymbol{Y}_j$, σ_n is the original noise variance, and $var(\cdot)$ is the variance operation. Then, the AWGF model is performed on the patch group $\boldsymbol{Y}_j$, where the weighted coefficient τ is set as $\tau = c\sigma_{n,j}^2$ with the coefficient c. Moreover, we obtain the graph eigenvectors $\boldsymbol{V}_g$ of Eq. (5) from the classical graph Laplacian matrix $\boldsymbol{L}$ [Meyer and Shen (2014)]. The corresponding restored patches $\left\{\boldsymbol{X}_j\right\}$ are achieved by calculating Eq. (10) and Eq. (5), which sequentially assemble the intermediate denoised image $\mathbf{X}^{(k)}$. We cast $\mathbf{X}^{(k)}$ in the next iteration to form the intermediate image $\mathbf{Y}^{(k+1)}$. Finally, the optimal denoised image $\tilde{\mathbf{X}}$ is obtained in the K-th iteration.

Algorithm 1 Image denoising by AWGF

Input: Noisy image $\mathbf{Y}$, noise variance σ_n.

1: Initialize intermediate noisy and denoised images with $\mathbf{Y}^{(0)} = \mathbf{X}^{(0)} = \mathbf{Y}$.
2: **For** $k = 1:K$ **do**
3: Set intermediate noisy image $\mathbf{Y}^{(k)} = \alpha\mathbf{X}^{(k-1)} + (1-\alpha)\mathbf{Y}$.
4: **For** each patch $\boldsymbol{y}_j$ of $\mathbf{Y}^{(k)}$ **do**
5: Find similar patches of $\boldsymbol{y}_j$ to form patch group $\boldsymbol{Y}_j$.
6: Calculate eigenvectors $\boldsymbol{V}_g$ of Laplacian matrix $\boldsymbol{L}$.
7: Estimate noise variance $\sigma_{n,j}$ by Eq. (11).
8: Get shrinkage coefficients $\left\{\tilde{\sigma}_{g,j}\right\}$ by Eq. (10).
9: Obtain restored patch group $\boldsymbol{X}_j$ by Eq. (5).
10: **end for**
11: Aggregate all $\left\{\boldsymbol{X}_j\right\}$ to form intermediate denoised image $\mathbf{X}^{(k)}$.
12: **end for**

Output: Optimal denoised image $\tilde{\mathbf{X}} = \mathbf{X}^{(K)}$.

3.2 Graph filtering explanation for ARLLR

We explain the ARLLR model from the graph filtering perspective. Problem Eq. (1) is first turned into a graph filtering form as

$$\left\{\tilde{\sigma}_{g,i}'\right\} = \arg\min_{\left\{\sigma_{g,i}'\right\}} \frac{1}{2\tau}\left\|\boldsymbol{Y} - \boldsymbol{Y}\boldsymbol{V}\boldsymbol{\Sigma}_g'\boldsymbol{V}^T\right\|_F^2 + \sum_{i=1}^{r} g\left(\sigma_{g,i}'\right), \tag{12}$$

where $\boldsymbol{\Sigma}_g'$ is a diagonal matrix with the shrinkage coefficients $\left\{\sigma_{g,i}'\right\}$. In Eq. (12), the singular value matrix of $\boldsymbol{X}$ is equal to $\boldsymbol{\Sigma}_x = \boldsymbol{\Sigma}_y\boldsymbol{\Sigma}_g'$ with its corresponding diagonal entries

$\sigma_{x,i} = \sigma_{y,i}\sigma'_{g,i}$. Comparing Eq. (12) with Eq. (4), the major difference lies in the number of used bases. Since the rank number r is usually smaller than the patch number N, we can build a full space supported by bases $\boldsymbol{V}_g = [\boldsymbol{V} \quad \boldsymbol{V}_\perp]$, where $\boldsymbol{V}_\perp$ is the orthogonal complement bases of $\boldsymbol{V}$. Once $\boldsymbol{V}$ is treated as the low frequency bases of $\boldsymbol{V}_g$, the shrinkage coefficients $\boldsymbol{\Sigma}'_g$ of ARLLR can be extended as $\boldsymbol{\Sigma}_g$ of Eq. (4) by padding zeros. By replacing the parameter pair $(\boldsymbol{V}, \boldsymbol{\Sigma}'_g)$ with $(\boldsymbol{V}_g, \boldsymbol{\Sigma}_g)$, problem Eq. (12) is rewritten as

$$\begin{aligned} \{\tilde{\sigma}_{g,i}\} = \arg\min_{\{\sigma_{g,i}\}} & \frac{1}{2\tau}\left\|\boldsymbol{Y} - \boldsymbol{Y}\boldsymbol{V}_g\boldsymbol{\Sigma}_g\boldsymbol{V}_g^T\right\|_F^2 + \sum_{i=1}^{r} g(\sigma_{g,i}), \\ s.t. \quad & \boldsymbol{Y} = \boldsymbol{Q}\boldsymbol{V}^T, \\ & \boldsymbol{V} \subseteq \boldsymbol{V}_g, \\ & 1 \le i \le r, \end{aligned} \tag{13}$$

where $\boldsymbol{Q}$ is the component coefficients of $\boldsymbol{Y}$ on $\boldsymbol{V}$ with $\boldsymbol{Q} = \boldsymbol{U}\boldsymbol{\Sigma}_y$. In the consideration of $g(\sigma_{g,i}) = log|\beta_i\sigma_{g,i} + \varepsilon|$ and $\beta_i = \sigma_{y,i}$, the final graph filtering form of ARLLR is provided as

$$\begin{aligned} \{\tilde{\sigma}_{g,i}\} = \arg\min_{\{\sigma_{g,i}\}} & \frac{1}{2\tau}\left\|\boldsymbol{Y} - \boldsymbol{Y}\boldsymbol{V}_g\boldsymbol{\Sigma}_g\boldsymbol{V}_g^T\right\|_F^2 + \sum_{i=1}^{r} |\sigma_{y,i}\sigma_{g,i} + \varepsilon|, \\ s.t. \quad & \boldsymbol{Y} = \boldsymbol{Q}\boldsymbol{V}^T, \\ & \boldsymbol{V} \subseteq \boldsymbol{V}_g, \\ & 1 \le i \le r. \end{aligned} \tag{14}$$

In Eq. (14), it shows the ARLLR model is a special form of AWGF, where it has two additional constraints. The noisy patch group $\boldsymbol{Y}$ is required to represent in a subspace of $\boldsymbol{V}_g$. Meanwhile, the optimization procedure is only performed on the first r shrinkage coefficients $\{\sigma_{g,i}\}$ with setting the rest coefficients zeros.

4 Experimental results

We compare the AWGF method with several state-of-the-art methods, including BM3D [Dabov, Foi, Katkovnik et al. (2007)], NCSR [Dong, Zhang, Shi et al. (2013)], ARLLR [Jia, Feng and Wang (2016a)] and denoising convolutional neural network (DnCNN) [Zhang, Zuo, Chen et al. (2016)]. Note that, the first three methods belong to the model-based methods, while the last one is a discriminative-learning-based method. Moreover, since our method is developed by ARLLR, the denoising parameters inherit from those in ARLLR. Some clean images are shown in Fig. 1 as test materials. Their noisy images are all generated by adding Gaussian noise.

We firstly give the denoised image comparison by our AWGF and three model-based methods in Fig. 2, where the noisy images contain the noise with its deviation $\sigma_n = 30$. It shows NCSR performs worst. Since NCSR employs sparse representation to directly extract the features from noisy patches, the learned atoms are inevitably contaminated by the noise. Consequently, it makes the description of image features ineffective and achieves the low denoising performance. BM3D is better than NCSR. Due to the jointed

filtering approach is used on similar patches, the features of patch group are robustly obtained to cope with the noise disturbance. ARLLR is the best. It shows the shrinkage of singular value is an efficient strategy to remove noise, for the noise is centralized into some small values. As a result, it is easy to wipe the noise by the shrinkage of singular value significance. As for AWGF, its performance is slightly worse than that of ARLLR. Though we introduce the shrinkage approach for the component coefficients in each graph frequency band, the optimal construction of graph filter is not referred. As mentioned in Algorithm 1, we simply build a graph filter from the traditional Laplacian matrix without any further consideration. However, AWGF still outperforms NCSR and BM3D, which shows the remarkable effect of graph filtering.

Figure 1: Clean images. From left to right on the top and bottom lines, images are named as C. Man, House, Peppers, Monarch, Lena, Barbara, Boat and Baboon

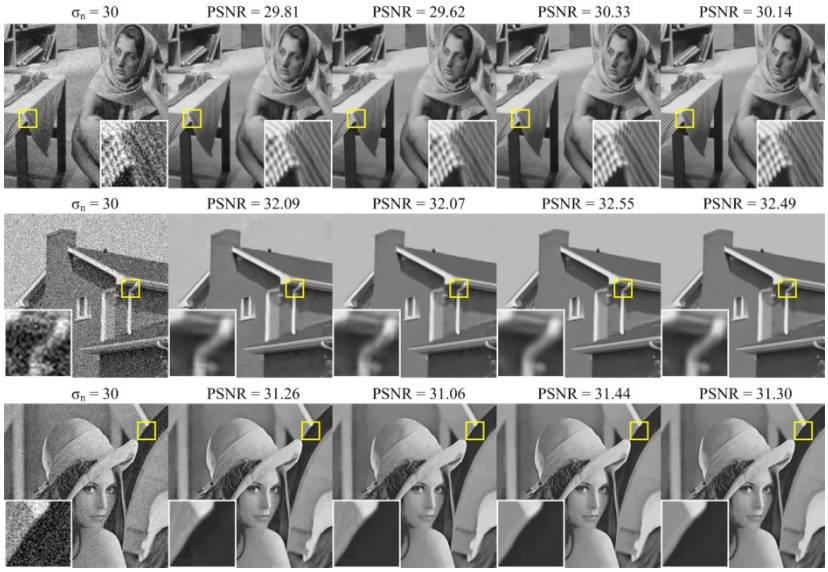

Figure 2: Denoised image comparison with PSNR (dB) in the noise deviation σ_n=30. From left to right are the noisy images and their corresponding denoised images by BM3D, NCSR, ARLLR and our AWGF, respectively

The denoised image comparison in the noise deviation of $\sigma_n = 50$ is provided in Fig. 3. The similar result is achieved as that in $\sigma_n = 30$. ARLLR and AWGF are better than BM3D and NCSR, where ARLLR has slight superiority over AWGF. In Fig. 3, ARLLR

and AWGF have the better image restoration in textures and flat regions, e.g., in Barbara and Lena. From the view of graph filtering, they both benefit from the graph frequency analysis, where they require the restored patches smoothing evolved on graphs. We also note that the edges of Lena in ARLLR suffer from the artificial noise. However, this phenomenon is relieved in AWGF, for the full space is used to restore clean images.

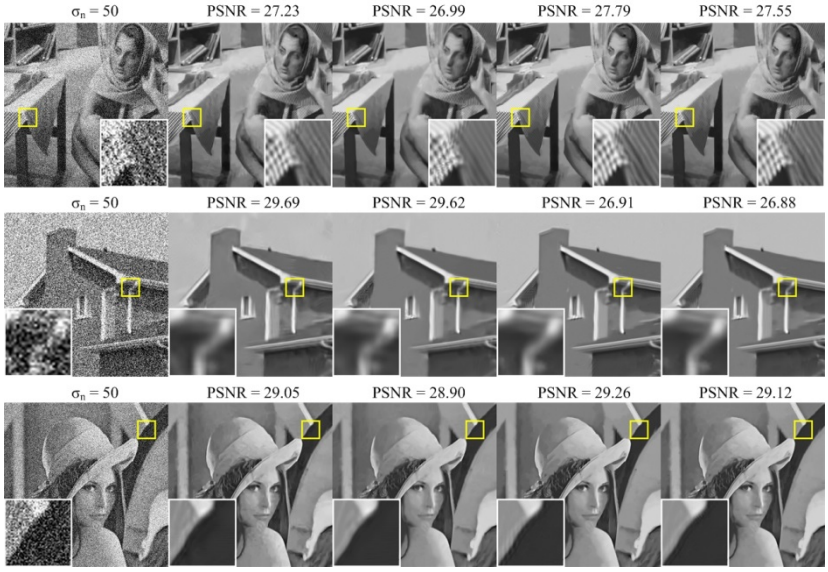

Figure 3: Denoised image comparison with PSNR (dB) in the noise deviation σ_n=50. From left to right are the noisy images and their corresponding denoised images by BM3D, NCSR, ARLLR and our AWGF, respectively

The statistical results of PSNR and SSIM are shown in Tabs. 1 and 2, where the DnCNN method is additional tested for comparison. We use BM3D as a baseline, since it achieves the acceptable performance for all images and noise levels. From Tabs. 1 and 2, it shows the denoising performance of NCSR is better than that of BM3D in the small noise of $\sigma_n = 10$ but worse in the noise of $\sigma_n \geq 30$. The learned features in atoms tend to be obscured by the large noise, due to the dictionary is directly trained from noisy images. ARLLR is better than the two former methods because of its singular value shrinkage strategy. DnCNN is best among all test methods. It utilizes the external prior of image databases rather than the internal prior from the noisy image itself. As for AWGF, it also has a remarkable performance in the noise of $\sigma_n \geq 30$. It is thanks to the adaptive shrinkage approach to get rid of the noise on all bands. However, AWGF is ineffective to deal with the small noise, which will be further discussed in the next experiment.

Table 1: PSNR (dB) results by different denoising methods

	$\sigma_n = 10$					$\sigma_n = 30$				
	BM3D	NCSR	ARLLR	DnCNN	AWGF	BM3D	NCSR	ARLLR	DnCNN	AWGF
C. Man	34.18	34.18	34.43	34.70	34.18	28.64	28.58	28.78	29.38	28.74
House	36.71	36.80	36.93	36.63	36.14	32.09	32.07	32.55	32.59	32.49

Peppers	34.68	34.68	34.95	35.04	34.05	29.28	29.10	29.49	29.98	29.44
Monarch	34.12	34.51	35.04	35.24	34.51	28.36	28.46	28.91	29.31	28.78
Lena	35.93	35.85	36.05	36.22	35.42	31.26	31.06	31.44	31.78	31.30
Barbara	34.98	35.00	35.52	34.65	34.58	29.81	29.62	30.33	29.11	30.14
Boat	33.92	33.91	34.08	34.08	33.71	29.12	28.93	29.23	29.46	29.15
Baboon	30.58	30.61	30.82	30.86	30.48	24.57	24.63	24.95	25.07	24.61
Average	**34.39**	**34.44**	**34.73**	**34.68**	**34.13**	**29.14**	**29.06**	**29.46**	**29.59**	**29.33**
			$\sigma_n = 50$					$\sigma_n = 100$		
C. Man	26.12	26.14	26.42	27.11	26.40	23.07	22.93	23.36	23.95	23.22
House	29.69	29.62	30.33	30.28	30.21	25.87	25.56	26.66	26.61	26.54
Peppers	26.68	26.65	26.91	27.39	26.88	23.39	22.84	23.45	23.91	23.37
Monarch	25.82	25.76	26.32	26.85	26.18	22.52	22.11	22.95	23.43	22.76
Lena	29.05	28.90	29.26	29.60	29.12	25.95	25.71	26.22	26.59	26.17
Barbara	27.23	26.99	27.79	26.38	27.55	23.62	23.20	24.37	22.72	24.18
Boat	26.78	26.66	26.97	27.27	26.83	23.97	23.68	24.11	24.46	23.95
Baboon	22.35	22.44	22.82	22.91	22.41	20.39	20.23	20.56	20.57	20.33
Average	**26.72**	**26.64**	**27.10**	**27.22**	**26.95**	**23.60**	**23.28**	**23.96**	**24.03**	**23.82**

Some images restored in the noise deviation σ_n=10 are shown in Fig. 4. The proposed AWGF is worst among all the test methods in the case of small noise. In AWGF, the flat regions of image suffer from more fluctuation of pixel value. As we know, flat regions are lack of features, which only contain the direct-current component. However, AWGF always tries to get the smoothed components from noisy patches. Once a threshold of noise variation is given, it inevitably extracts some artificial smoothed components from noisy patches, due to these components are also under the control of noise threshold. Since they are something different from the direct-current component, it deteriorates the denoising performance of flat regions. On the other hand, our graph filter is generated from the traditional Laplacian matrix. This graph filter is without any optimization such that its used bases are not the smoothest ones for filtering. It also affects the denoised images with more pixel fluctuation.

Table 2: SSIM results by different denoising methods

			$\sigma_n = 10$					$\sigma_n = 30$		
	BM3D	NCSR	ARLLR	DnCNN	AWGF	BM3D	NCSR	ARLLR	DnCNN	AWGF
C. Man	0.9300	0.9312	0.9319	0.9361	0.9282	0.8308	0.8392	0.8338	0.8551	0.8380
House	0.9234	0.9238	0.9244	0.9152	0.9142	0.8500	0.8487	0.8543	0.8576	0.8530
Peppers	0.9303	0.9272	0.9321	0.9342	0.9239	0.8528	0.8501	0.8587	0.8721	0.8567
Monarch	0.9549	0.9572	0.9592	0.9624	0.9516	0.8808	0.8855	0.8915	0.9030	0.8905
Lena	0.9165	0.9167	0.9177	0.9201	0.9094	0.8456	0.8455	0.8519	0.8608	0.8491
Barbara	0.9412	0.9416	0.9438	0.9406	0.9341	0.8673	0.8670	0.8801	0.8570	0.8784

Boat	0.8877	0.8883	0.8897	0.8904	0.8902	0.7782	0.7715	0.7791	0.7892	0.7773
Baboon	0.8982	0.8925	0.9045	0.9073	0.9023	0.7034	0.6964	0.7305	0.7389	0.6978
Average	**0.9228**	**0.9223**	**0.9254**	**0.9284**	**0.9192**	**0.8261**	**0.8255**	**0.8350**	**0.8417**	**0.8301**
			$\sigma_n = 50$					$\sigma_n = 100$		
C. Man	0.7764	0.7835	0.7791	0.8005	0.7880	0.6880	0.7060	0.6934	0.7289	0.7035
House	0.8146	0.8161	0.8244	0.8289	0.8245	0.7229	0.7407	0.7545	0.7611	0.7575
Peppers	0.7939	0.8006	0.8020	0.8177	0.8015	0.6832	0.7054	0.6935	0.7193	0.6995
Monarch	0.8197	0.8260	0.8342	0.8506	0.8320	0.7017	0.7120	0.7266	0.7492	0.7234
Lena	0.8007	0.8035	0.8081	0.8211	0.8053	0.7109	0.7276	0.7294	0.7492	0.7306
Barbara	0.7932	0.7892	0.8187	0.7722	0.8143	0.6417	0.6389	0.6838	0.6073	0.6819
Boat	0.7042	0.6972	0.7069	0.7209	0.7067	0.5923	0.5930	0.5970	0.6195	0.5939
Baboon	0.5506	0.5493	0.6125	0.6145	0.5573	0.3820	0.3865	0.4094	0.3991	0.3722
Average	**0.7567**	**0.7582**	**0.7732**	**0.7783**	**0.7662**	**0.6403**	**0.6513**	**0.6610**	**0.6667**	**0.6578**

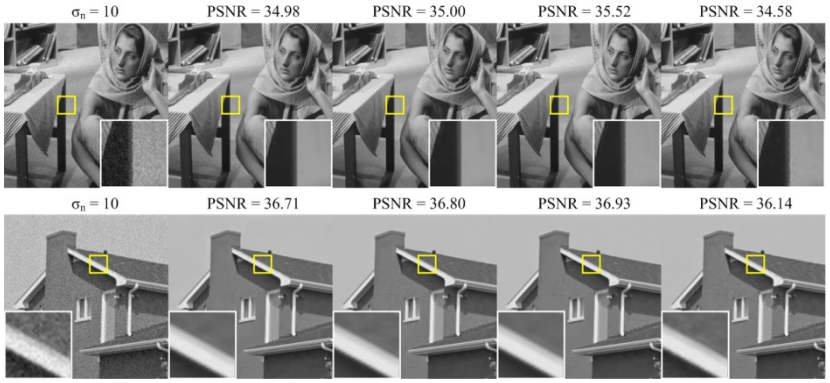

Figure 4: Denoised image comparison with PSNR (dB) in the noise deviation σ_n=10. From left to right are the noisy images and their corresponding denoised images by BM3D, NCSR, ARLLR and our AWGF, respectively

5 Conclusion

We propose an adaptive weighted graph filtering method for image denoising. Unlike the traditional ideal lowpass graph filtering, the proposed AWGF method adaptively shrinks the components in all graph frequency bands with their component significances. It makes the graph filtering more explainable and suitable for denoising. Moreover, we demonstrate the existing ARLLR method is a special form of graph filtering, which is under the constraint of subspace representation. It not only enriches the theory of graph filtering, but also builds a bridge from the low-rank methods to our graph filtering method. Experiments show the AWGF method achieves a comparable denoising performance with several state-of-the-art methods. However, AWGF is somewhat ineffective to tackle noisy images of small noise. It becomes our future work to overcome this problem by learning the optimal graph filter.

Acknowledgement: We thank Associate Professor Yuan Gao (University of Sydney, Australia) for her feedback on an earlier version of the manuscript.

Funding Statement: This work is supported by National Natural Science Foundation of China [61673108, 41706103]. The initials of authors who received these grants are LZ and YZ, respectively. It is also supported by Natural Science Foundation of Jiangsu Province, China [BK20170306]. The initials of author who received this grant are YZ.

Conflicts of Interest: The authors declare that they have no conflicts of interest to report regarding the present study.

References

Buades, A.; Coll, B.; Morel, J. M. (2005): A review of image denoising algorithms, with a new one. *Multiscale Modeling & Simulation*, vol. 4, no. 2, pp. 490-530.

Chen, Y.; Tang, Y.; Xu, N.; Zhou, L.; Zhao, L. (2016): Image denoising via adaptive eigenvectors of graph Laplacian. *Journal of Electronic Imaging*, vol. 25, no. 4, pp. 043019.

Chen, Y. T.; Wang, J.; Liu, S. J.; Chen, X.; Xiong, J. et al. (2019): Multiscale fast correlation filtering tracking algorithm based on a feature fusion model. *Concurrency and Computation: Practice and Experience*, pp. e5533.

Dabov, K.; Foi, A.; Katkovnik, V.; Egiazarian, K. (2007): Image denoising by sparse 3-D transform-domain collaborative filtering. *IEEE Transactions on Image Processing*, vol. 16, no. 8, pp. 2080-2095.

Deivalakshmi, S.; Palanisamy, P.; Gao, X. Z. (2019): Balanced GHM mutiwavelet transform based contrast enhancement technique for dark images using dynamic stochastic resonance. *Intelligent Automation and Soft Computing*, vol. 25, no. 3, pp. 459-471.

Dong, W.; Shi, G.; Li, X. (2013): Nonlocal image restoration with bilateral variance estimation: a low-rank approach. *IEEE Transactions on Image Processing*, vol. 22, no. 2, pp. 700-711.

Dong, W.; Zhang, L.; Shi, G.; Li, X. (2013): Nonlocally centralized sparse representation for image restoration. *IEEE Transactions on Image Processing*, vol. 22, no. 4, pp. 1620-1630.

Elad, M.; Aharon, M. (2006): Image denoising via learned dictionaries and sparse representation. *IEEE Conference on Computer Vision and Pattern Recognition*, pp. 895-900.

Hein, M.; Audibert, J. Y.; Luxburg, U. V. (2005): From graphs to manifolds—weak and strong pointwise consistency of graph Laplacians. *Conference on Learning Theory*, pp. 470-485.

Hu, Y.; Zhang, D.; Ye, J.; Li, X.; He, X. (2013): Fast and accurate matrix completion via truncated nuclear norm regularization. *IEEE Transactions on Pattern Analysis and Machine Intelligence*, vol. 35, no. 9, pp. 2117-2130.

Huang, T.; Dong, W.; Xie, X.; Shi, G.; Bai, X. (2017): Mixed noise removal via Laplacian scale mixture modeling and nonlocal low-rank approximation. *IEEE Transactions on Image Processing*, vol. 26, no. 7, pp. 3171-3186.

Jia, X.; Feng, X.; Wang, W. (2016a): Adaptive regularizer learning for low rank approximation with application to image denoising. *IEEE International Conference on Image Processing*, pp. 3096-3100.

Jia, X.; Feng, X.; Wang, W. (2016b): Rank constrained nuclear norm minimization with application to image denoising. *Signal Processing*, vol. 129, pp. 1-11.

Jia, X.; Liu, S.; Feng, X.; Zhang, L. (2019): FOCNet: a fractional optimal control network for image denoising. *IEEE Conference on Computer Vision and Pattern Recognition*, pp. 6047-6056.

Liu, H.; Xiong, R.; Liu, D.; Ma, S.; Wu, F. et al. (2018): Image denoising via low rank regularization exploiting intra and inter patch correlation. *IEEE Transactions on Circuits and Systems for Video Technology*, vol. 28, no. 12, pp. 3321-3332.

Liu, L.; Chen, L.; Chen, C. L. P.; Tang, Y. Y.; Pun, C. M. (2017): Weighted joint sparse representation for removing mixed noise in image. *IEEE Transactions on Cybernetics*, vol. 47, no. 3, pp. 600-611.

Mäkinen, Y.; Azzari, L.; Foi, A. (2019): Exact transform-domain noise variance for collaborative filtering of stationary correlated noise. *IEEE International Conference on Image Processing*, pp. 185-189.

Meyer, F. G.; Shen, X. (2014): Perturbation of the eigenvectors of the graph Laplacian: application to image denoising. *Applied and Computational Harmonic Analysis*, vol. 36, no. 2, pp. 326-334.

Pang, J.; Cheung, G. (2017): Graph Laplacian regularization for image denoising: analysis in the continuous domain. *IEEE Transactions on Image Process*, vol. 26, no. 4, pp. 1770-1785.

Shao, L.; Yan, R.; Li, X.; Liu, Y. (2017): From heuristic optimization to dictionary learning: a review and comprehensive comparison of image denoising algorithms. *IEEE Transactions on Cybernetics*, vol. 44, no. 7, pp. 1001-1013.

Talebi, H.; Milanfar, P. (2014): Global image denoising. *IEEE Transactions on Image Processing*, vol. 23, no. 2, pp. 755-768.

Tang, Y.; Chen, Y.; Xu, N.; Jiang, A.; Zhou, L. (2016): Image denoising via sparse coding using eigenvectors of graph Laplacian. *Digital Signal Processing*, vol. 50, pp. 114-122.

Tessens, L.; Pizurica, A.; Alecu, A.; Munteanu, A; Philips, W. R. (2008): Context adaptive image denoising through modeling of curvelet domain statistics. *Journal of Electronic Imaging*, vol. 17, no. 3, pp. 033021.

Verma, R.; Pandey, R. (2017): Adaptive selection of search region for NLM based image denoising. *Optik*, vol. 147, pp. 151-162.

Wang, H.; Cen, Y.; He, Z.; He, Z.; Zhao, R. et al. (2018): Reweighted low-rank matrix analysis with structural smoothness for image denoising. *IEEE Transactions on Image Processing*, vol. 27, no. 4, pp. 1777-1792.

Waheed, W.; Tay, D. (2018): Graph polynomial filter for signal denoising. *IET Signal Processing*, vol. 12, no. 3, pp. 301-309.

Wang, J.; Cai, J.; Shi, Y.; Yin, B. (2015): Incoherent dictionary learning for sparse representation-based image denoising. *IEEE International Conference on Image Processing*, pp. 4582-4586.

Wang, W.; Jiang, Y. B.; Luo, Y. H.; Li, J.; Wang, X. et al. (2019): An advanced deep residual dense network approach for image super-resolution. *International Journal of Computational Intelligence Systems*, vol. 12, no. 2, pp. 1592-1601.

Wu, Q.; Li, Y.; Lin, Y.; Zhou, R. (2018): Weighted sparse image classification based on low rank representation. *Computers, Materials & Continua*, vol. 56, no. 1, pp. 91-105.

Yan, R.; Shao, L.; Liu, Y. (2013): Nonlocal hierarchical dictionary learning using wavelets for image denoising. *IEEE Transactions on Image Processing*, vol. 22, no. 12, pp. 4689-4698.

Yang, Z.; Fan, L.; Yang, Y.; Yang, Z.; Gui, G. (2019): Generalized singular value thresholding operator based nonconvex low-rank and sparse decomposition for moving object detection. *Journal of The Franklin Institute*, vol. 356, no. 16, pp. 10138-10154.

Yang, Z.; Yang, Z.; Han, D. (2018): Alternating direction method of multipliers for sparse and low-rank decomposition based on nonconvex non-smooth weighted nuclear norm. *IEEE Access*, vol. 6, no. 1, pp. 56945-56953.

Zeng, X.; Bian, W.; Liu, W.; Shen, J.; Tao, D. (2015): Dictionary pair learning on Grassmann manifolds for image denoising. *IEEE Transactions on Image Processing*, vol. 24, no. 11, pp. 4556-4569.

Zha, Z.; Zhang, X.; Wang, Q.; Bai, Y.; Chen, Y. et al. (2018): Group sparsity residual constraint for image denoising with external nonlocal self-similarity prior. *Neurocomputing*, vol. 275, pp. 2294-2306.

Zhang, H.; He, W.; Zhang, L.; Shen, H.; Yuan, Q. (2014): Hyperspectral image restoration using low-rank matrix recovery. *IEEE Transactions on Geoscience and Remote Sensing*, vol. 52, no. 8, pp. 4729-4743.

Zhang, K.; Zuo, W.; Chen, Y.; Meng, D.; Zhang, L. (2016): Beyond a Gaussian denoiser: residual learning of deep CNN for image denoising. *IEEE Transactions on Image Processing*, vol. 26, no. 7, pp. 3142-3155.

Zhang, K.; Zuo, W.; Zhang, L. (2018): FFDNet: toward a fast and flexible solution for CNN based image denoising. *IEEE Transactions on Image Processing*, vol. 27, no. 9, pp. 4608-4622.

Zhang, M.; Gunturk, B. K. (2008): Multiresolution bilateral filtering for image denoising. *IEEE Transactions on Image Processing*, vol. 17, no. 12, pp. 2324-2333.